MUON BEAM HELICAL COOLING CHANNEL DESIGN*

R. P. Johnson[#], C. M. Ankenbrandt, G. Flanagan, G. M. Kazakevich, F. Marhauser,
M. Neubauer, T. J. Roberts, C. Yoshikawa, Muons, Inc., Batavia, IL, USA
Y. S. Derbenev, V. S. Morozov, Jefferson Lab, Newport News, VA, USA
V. S. Kashikhin, M. L. Lopes, A. Tollestrup, K. Yonehara, A. Zlobin, Fermilab, Batavia, IL, USA

Abstract

The Helical Cooling Channel (HCC) achieves effective ionization cooling of the six-dimensional (6d) phase space of a muon beam by means of a series of 21st century inventions. In the HCC, hydrogen-pressurized RF cavities enable high RF gradients in strong external magnetic fields. The theory of the HCC, which requires a magnetic field with solenoid, helical dipole, and helical quadrupole components, demonstrates that dispersion in the gaseous hydrogen energy absorber provides effective emittance exchange to enable longitudinal ionization cooling. The 10-year development of a practical implementation of a muon-beam cooling device has involved a series of technical innovations and experiments that imply that an HCC of less than 300 m length can cool the 6d emittance of a muon beam by six orders of magnitude. We describe the design and construction plans for a prototype HCC module based on oxygen-doped hydrogen-pressurized RF cavities that are loaded with dielectric, fed by magnetrons, and operate in a superconducting helical solenoid magnet.

OVERVIEW

Much of the ionization cooling technology included in the conceptual design discussed here did not exist before this millennium. Below we describe these new technologies and their verification by calculations, simulations, and experiments. We present a conceptual design of a module of an HCC that demonstrates how to marry the new concepts into a practical cooling channel to enable muon colliders and to make muon beams for neutrino factories and precision experiments affordable.

The design incorporates the HCC theory with emittance exchange using a continuous absorber [1], hydrogen-pressurized RF cavities [2] loaded with dielectric [3] and doped with oxygen [4], Helical Solenoid (HS) magnets [5], phase and frequency-locked magnetron power sources [6], and optimizations using G4beamline [7] muon beam cooling simulations. The innovations that were developed with support from the DOE SBIR-STTR program are combined to provide a practical engineering solution for a muon-beam cooling channel. The references above indicate the many contributors and institutions to the conception, development, and verification of the HCC and its components.

In the description that follows, six segments, each with the same parameters, form a 233 m long linear magnetic channel. Each segment is composed of modules that are similar to the prototype module described here.

HCC THEORY

The theory of the Helical Cooling Channel, extended to include a continuous homogeneous absorber, provides a framework to develop practical devices and techniques. The forces generated by particle motion in combined solenoid and Siberian-snake helical dipole fields are used to construct a Hamiltonian that is solved by moving into the rotating frame of the helical dipole where stability requirements determine the need for a helical quadrupole.

In an HCC, solenoid and transverse helical dipole field components provide a constant dispersion along the channel for emittance exchange to allow longitudinal cooling. The helical dipole component creates an outward radial force due to the longitudinal momentum of the particle while the solenoid component creates an inward radial force due to the transverse momentum of the particle:

$$F_{h-dipole} \approx p_z \times b; \quad b \equiv B_\perp; \qquad F_{solenoid} \approx -p_\perp \times B; \quad B \equiv B_z,$$

where B is the solenoid component, the axis of which defines the z axis, and b is the transverse helical dipole field component. Figure 1 shows the motion of particles around the equilibrium orbit (red).
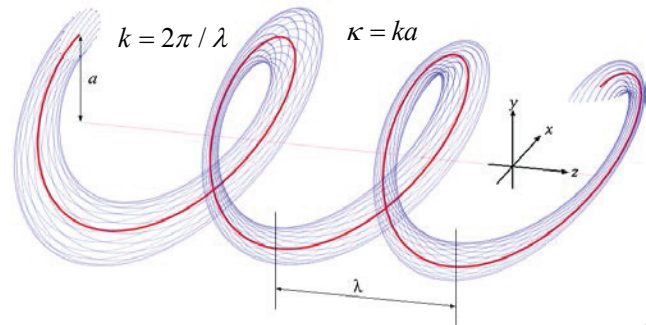

Figure 1: Schematic of beam motion in an HCC. Unlike cooling in a solenoid, the radius, a, does not diminish.

The equilibrium orbit shown in red follows the equation that is the Hamiltonian solution:

$$p(a) = \frac{\sqrt{1+\kappa^2}}{k}\left[B - \frac{1+\kappa^2}{\kappa} b \right] \qquad (1)$$

The dispersion factor $\hat{D}$ is determined by the field components B, b, and the transverse magnetic field radial gradient $\partial b/\partial a$ on the particle orbit:

$$\hat{D} = \frac{p}{a}\frac{da}{dp} = \left(\frac{a}{p}\frac{dp}{da}\right)^{-1}; \qquad \hat{D}^{-1} = \frac{\kappa^2 + (1-\kappa^2)q}{1+\kappa^2} + g; \qquad g \equiv \frac{-(1+\kappa^2)^{3/2}}{pk^2}\frac{\partial b}{\partial a},$$

where g is the effective field index at the periodic orbit.

The magnetic field ratio on the equilibrium trajectory satisfies the condition

$$\frac{b}{B} = \frac{\kappa}{1+\kappa^2}\left(1 - \frac{k}{k_c}\right) = \frac{\kappa}{1+\kappa^2}\left(\frac{q}{q+1}\right), \text{ where } q \equiv \frac{k_c}{k} - 1.$$

For stability, the following condition has to be satisfied

$$0 \; < \; G \equiv (q-g)\hat{D}^{-1} \; < \; R^2 \equiv \frac{1}{4}\left(1+\frac{q^2}{1+\kappa^2}\right)^2 . \quad (2)$$

The solutions for the HCC magnet system demonstrate transverse stability with 40,000 mm-mr normalized transverse acceptance in each plane, confirmed by G4beamline numerical simulations. The theoretical framework has allowed the development of emittance-preserving matching-sections between HCC segments and the exploitation of a transition gamma to optimize RF bucket parameters to increase longitudinal acceptance.

HCC SIMULATIONS

A series of six HCC segments [8] that reduces the 6d emittance of a 200 MeV/c beam by a factor of 175,000 is presented in Table 1 and shown graphically in Figure 2. Segment 4 is shorter by 40 m than previously reported, reflecting recent innovations to match the emittances between segment transitions involving changes in RF frequency and/or HCC magnet parameters [9].

Table 1: 6-segment HCC as Simulated by G4beamline

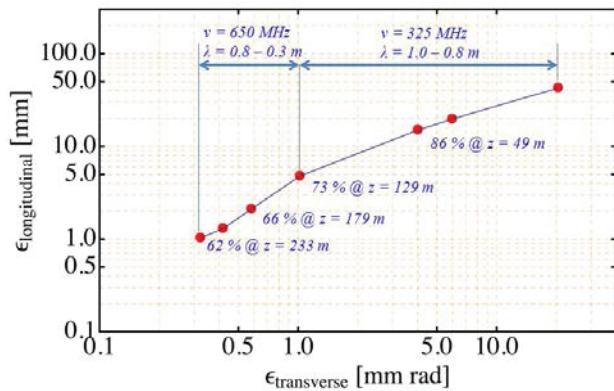| segment	z	b	db/da	B	λ	ν	ε_T	ε_L	ε_{6D}	μ/μ_t
	m	T	T/m	T	m	MHz	mm	mm	mm^3	%
start	0	1.3	-0.5	-4.2	1	325	20.4	42.8	12,900	100
1	40	1.3	-0.5	-4.2	1	325	5.97	19.7	415.9	92
2	49	1.4	-0.6	-4.8	0.9	325	4.01	15	108	86
3	129	1.7	-0.8	-5.2	0.8	325	1.02	4.8	3.2	73
4	179	2.6	-2	-8.5	0.5	650	0.58	2.1	2	66
5	203	3.2	-3.1	-9.8	0.4	650	0.42	1.3	0.14	64
6	233	4.3	-5.6	-14.1	0.3	650	0.32	1	0.08	62

Figure 2: Emittance evolution and muon survival for the six HCC segments shown in Table 1.

The two transverse emittances (the average is shown) and one longitudinal emittance must be reduced to allow affordable acceleration for a neutrino factory or muon collider. In this example, 38% of the muons are lost due to muon decay and scraping. The beam after Segment 6 is suitable for a neutrino factory, precision muon experiments like mu2e or g-2, for cargo scanning, or a muon collider Higgs factory, where ε_L=1 mm corresponds to the expected 4 MeV width of the standard model Higgs boson. Highest luminosity Higgs or energy-frontier muon colliders need additional transverse cooling.

HCC ENGINEERING DESIGN

Figure 3 shows the essential features of a compact design of an HCC module where hydrogen-pressurized, dielectric-loaded RF cavities fit inside HS magnet coils. In this concept, the HS magnet and its 4 K cryostat are thermodynamically independent of the RF cavities and their power sources. Figure 4 shows a cut-away view of a module with 20 RF cavities that could be the first device to be built and tested. Figure 5 shows a three-dimensional view of the same module.
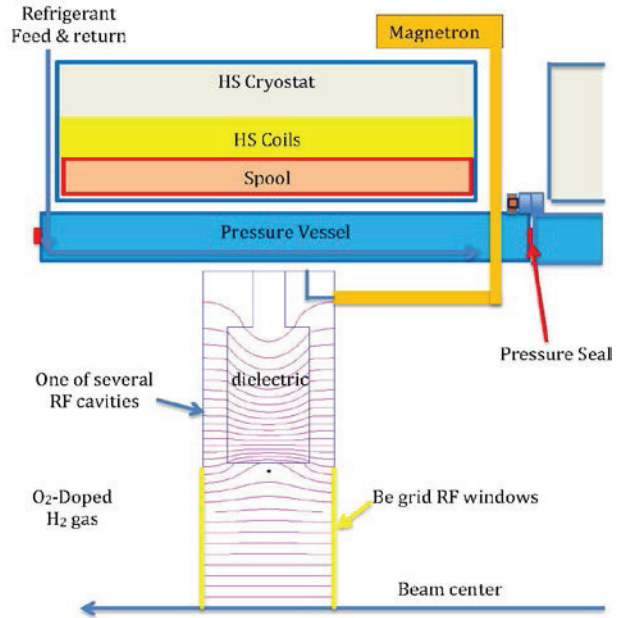

Figure 3: Conceptual diagram showing the features of a beam-cooling module with dielectric-loaded RF cavities, Be RF windows, pressure vessel, HS coil, and its cryostat.
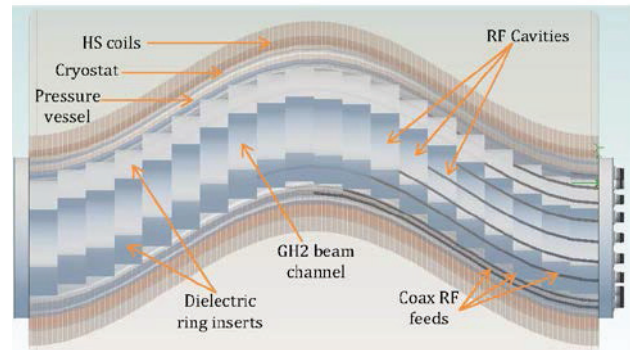

Figure 4: Conceptual diagram of an HCC module, showing dielectric-loaded RF cavities enclosed in a pressure vessel that "screws" into the HS cryostat. The pressure vessel contains tubes for water or LN2 refrigerant.

The coax feed for each cavity comes from a magnetron power source fed through a break in the magnet structure where the magnet cryostats end. The pressure vessel wall is refrigerated by circulating liquid or gas (water, LN2, or gaseous Helium), and could be machined to contain the

coax power leads. Compared to earlier design concepts, this one has only one break between coils per module and no penetrations of the cryostat by RF feeds.
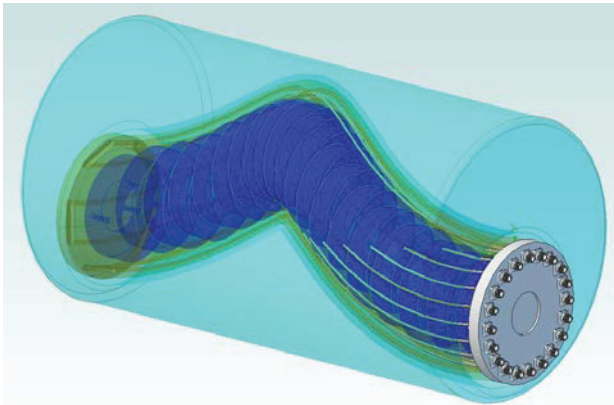

Figure 5: Three-dimensional visualization of Figure 4.

In the following sections, we discuss the motivation, design details, and experimental verification of the components of the module design.

H$_2$-PRESSURIZED RF CAVITIES

As the most effective ionization-cooling energy-absorber material, having the largest product of dE/dx and radiation length, hydrogen offers several other benefits in pressurized RF cavities, allowing:

a) Higher accelerating gradients by suppressing RF breakdown even in high magnetic fields;

b) The energy absorber and RF energy regeneration to occupy the same real estate to shorten the cooling channel;

c) A new kind of emittance exchange where momentum-dependent path length in the continuous, homogeneous hydrogen energy absorber provides the required correlation to cool in six dimensions;

d) Heat removal from the cavities themselves by virtue of having the highest heat capacity and lowest viscosity of all gases;

e) Heat removal from the low-Z beryllium gridded windows to eliminate the irises of the RF cavities such that the accelerating field in the pillbox cavity is as high as the maximum surface field.

Pressurized RF cavity accomplishments include:

a) Experimental verification that maximum RF fields are not affected by strong external magnetic fields [10];

b) Calculations and simulations [11] of RF energy absorption due to beam-induced ionization;

b) Experimental demonstration of SF$_6$ and oxygen as effective dopants to mitigate beam-induced plasma loading and Q loss [12];

c) First test of a dielectric insert to reduce cavity diameter at a given frequency showing that high-pressure gas suppresses RF breakdown of dielectric surfaces [13];

d) Development of inexpensive, efficient, phase and frequency-locked magnetrons power sources [14].

HELICAL SOLENOID (HS) MAGNET

The invention of the Helical Solenoid (HS) magnet provides a simple configuration of coils to generate the solenoid, helical dipole, and helical quadrupole field components required for the HCC. The HS overcame the difficulty of very high coil currents required to produce the quadrupole field component in an ordinary magnet design. Note that the HS is not a bent solenoid. In a HS the coil planes are normal to the z axis, while a bent solenoid would have the coil planes normal to the equilibrium orbit.
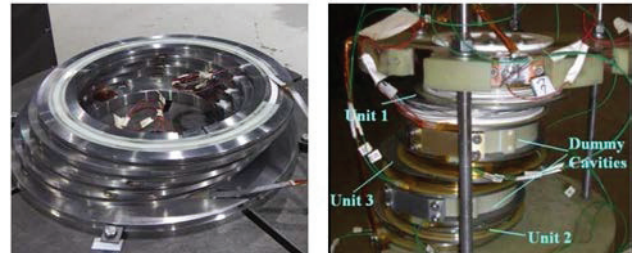

Figure 6: Previous HS fabrication projects: (left) NbTi HS [15] and (right) YBCO HS [16].

Multi-coil HS magnet sections have been designed, constructed, and tested as shown in Figure 6 using NbTi for the lowest field (5T, four coil) and YBCO for the highest field (15 T, 6 coil) HCC segments. The coil design for the intermediate HCC section (10 T, continuous coil) is being made to provide a technology demonstration and develop practical experience with the construction and performance of a Nb$_3$Sn helical solenoid.

In the design shown in Figures 1 through 3, the RF cavities in their continuous pressure vessel fit inside the HS spool and cryostat, which has a slightly larger inner radius than the pressure vessel. Figure 7 shows a model of the new continuous coil configuration of the HS wound on a spool that will fit around the pressure vessel.

Figure 7: Conceptual drawing (left) and 3d printer version (right) of the Nb$_3$Sn HS spool and conductor that will be fabricated and tested in the Fermilab Vertical Magnet Test Facility. The test will use two layers of cable.

DIELECTRIC LOADED RF CAVITIES

Dielectric loaded RF cavities reduce the transverse size of the RF cavities to allow them to fit inside the HS coils. The cavity offsets shown in Figure 8 allow coaxial power feeds to enter the sides of the cavities such that the distribution system is inside the hydrogen pressure volume. The cavities are entirely inside of the pressure vessel so their walls are not gas pressure bearing and do not require strength beyond that needed for normal construction and handling. Convection by the pressurized hydrogen gas from the refrigerated pressure vessel keeps the cavities at constant temperature. All cavities must be tuned to the same frequency during construction. Temperature and hydrogen gas-pressure feedback systems (using the density dependence of the dielectric constant of hydrogen) lock the cavity frequency to the power source frequency during operation.

The HS magnet achieves the required ratios of solenoid, helical dipole, and helical quadrupole field components by having the correct dimensions of the coils. For the best performance, the RF bucket needs to be larger and RF frequency lower than can be provided by a pillbox cavity that fits inside the HS coils. We have looked at several solutions to place lower frequency cavities inside the magnet that involve placing the HS coils between the cavities, using correction coils to modify the field, or changing the circular shape of the HS coils to be elliptical. In each case, these solutions, while possible, lead to larger structures that imply a larger magnet system with higher stored energy and expense that increase as the square of the HS inner radius.

A better solution is to add a dielectric inside the RF cavities to reduce their diameter for a given (lower) frequency such that they can fit inside the HS coils. High-pressure hydrogen gas will suppress surface breakdown of inserted dielectrics just as it suppresses breakdown of the cavities themselves at high gradient in a strong external field. First tests of an alumina dielectric in a pressurized cavity show promising results in that GH2 suppressed breakdown up to the point that the dielectric strength of the dielectric was reached.

For the required lower frequency, the cavity diameter can be small enough to allow coaxial power feeds to fit inside the pressure vessel containing the cavities. These coax feeds will also be filled with pressurized hydrogen such that they can have small diameters.

Previous simulations have shown the admittance of an HCC are determined from the strength of the magnetic fields and the RF frequency that can be used to contain the beam longitudinally. This imposes strict dimensional constraints for the RF cavities embedded within the magnetic system of the HCC. The use of gas-filled conventional pillbox cavities yields prohibitively large radii. Therefore, we load each cavity with ceramic material to reduce the radial size to tolerable values at the given (L-Band) frequency, corresponding to the HCC segment under consideration. To find an optimum RF cavity and engineering design, we have performed rigorous numerical investigations for cavities loaded with various ceramic shapes revealing quantitative relationships of critical RF operational parameters taking into account temperature-dependent material properties. The study particularly yields absolute input peak power and thermal power levels that can be expected at any operating temperature. We considered a range from room temperature down to ~33 K for the cavity operation. This lower limit is the critical temperature of hydrogen, where it will not liquefy at any pressure.
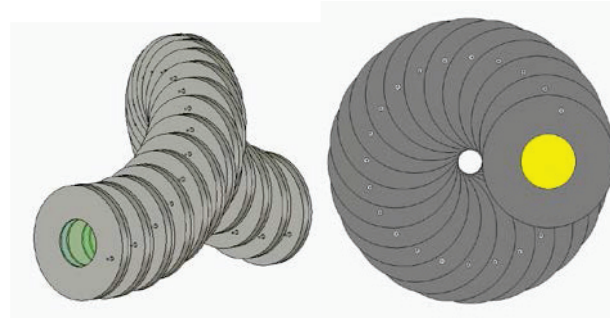

Figure 8: (Left) Illustration of RF cavities aligned to fit inside a HS magnet and cryostat. (Right) The end view shows the dielectric-filled region of the cavity (gray), where the yellow area corresponds to the region that the beam passes through. The small holes indicate the locations of the power feeds. Beryllium grids separate the cavities to make them RF pillboxes while not impeding oxygen-doped hydrogen flow.

MAGNETRON POWER SOURCES

A major design objective is to lower the required peak power (P_{peak}) level to sustain the envisaged effective field levels while employing contemporary, affordable, pulsed (μs pulse length) magnetron power sources. Such magnetron sources typically provide several ten to several hundred kW at L-Band frequencies. This is much smaller than the cavities would require for operation at a typical active length of $L_{act} = \beta\lambda/2$, with $\beta = v_\mu/c$ denoting the normalized muon velocity and $\lambda = c/f$ the RF wavelength (c = speed of light, f = frequency). Consequently, the peak power can only be diminished by a significant reduction of L_{act}. In fact, multiple rather short cavity cells (few centimeters long) fit into our proposed scheme to position cavities smoothly along the helical equilibrium orbit, thereby providing optimum replenishment of the longitudinal particle momentum lost during ionization cooling. Using affordable power sources, the cavities then can be powered separately providing each an optimum phase for acceleration. Moreover, the transit-time factor along the short L_{act} is close to unity for 200 to 250 MeV/c muon beams.

The cooling demand per cavity cell is relatively low (less than 1 kW), With this dielectric-loaded cavity solution, the coaxial feed for each of the cavities in an HCC unit can run inside the pressure vessel from the cavity to the gap between magnet cryostats where they

exit the pressure vessel and extend radially to power sources.

Phase and frequency locked magnetron power sources are especially attractive for any muon cooling channel. Ionization cooling achieves at best a 1/e emittance reduction in each transverse plane for every loss of energy equal to the beam energy. To get a factor of a million in 6d emittance reduction then requires energy replenishment approximately equal to 7 times the energy of the muon. Cooling at 250 MeV implies an equivalent accelerator of 1.75 GeV, something that for a conventional accelerator is in the $1B class for each muon charge unless the costs can be reduced significantly.

Magnetron power sources have the potential to cost $1 to $2/W compared to klystrons or IOTs at $5 to $10/W. They are also more efficient with typical values of 85% compared to 60% or less for the other sources. Muons, Inc. is working with Fermilab and Jefferson Lab to develop magnetrons for other accelerators, including their use as power sources for superconducting RF. Combining the outputs of two phase and frequency locked kitchen oven magnetrons to control microphonics demonstrated the needed techniques for the HCC application [14].

The RF requirements for the HCC are well suited to magnetron sources in that phase and frequency requirements are not as stringent as for other applications. The HCC normal-conducting RF system has Q > 20,000 at the temperatures of interest and the synchronous phase angle is small to allow large longitudinal acceptance.

SIMULATIONS AND OPTIMIZATION

The effect on the beam cooling performance of the gaps between HS coils and cryostats needed for connecting modules, feeding the RF power, and refrigerating the pressure vessel is partially known from earlier studies that showed little sensitivity for 5 cm gaps. However, the engineering solutions are just being developed to include practical constraints such as safety and maintainability. It is likely that a larger gap can be accommodated, at least in part, by having increased fields at the end of the modules. This study will be part of a larger study of field error tolerances.

The G4beamline and ICOOL simulation codes now operate on supercomputers for faster optimization of the systems described above. Active investigations include cooling at lower muon beam energy, matching emittances to reduce losses between segments, and matching emittances between cooling channels that follow or precede the 6 HCC segments described in Table 1.

An essential next step is to design an experiment using a muon beam based on the module described here to demonstrate effective, affordable 6d cooling. Demonstrating the technology of such a cooling channel would represent great progress towards muon-based accelerator technologies needed for the next energy frontier machines, neutrino factories, Higgs factories, precision muon experiments and commercial applications such as cargo scanning and muon spin resonance.

REFERENCES

[1] Y.S. Derbenev and R.P. Johnson, Phys. Rev. ST – Accelerators and Beams 8 (2005) 041002

[2] R.P. Johnson R.E. Hartline, C.M. Ankenbrandt, M. Kuchnir, A. Moretti, M. Popovic, M. Alsharo'a, E. L. Black, K. Cassel, D.M. Kaplan, A. V. Obabko, T. J. Roberts, AIP Conf. Proc. No. 671 (New York, 2003), pp.328 – 335

[3] G. Flanagan, R.P. Johnson, G. Kazakevich, F. Marhauser, M. Neubauer, V.S. Kashikin, M.L. Lopes, G. Romanov, M. Tartaglia, K. Yonehara, M. Yu, A.V. Zlobin, IPAC12, New Orleans, TUPPD010

[4] B. Freemire, P.M. Hanlet, Y. Torun, M. Chung, M.R. Jana, M. Leonova, A. Moretti, T.A. Schwarz, A.V. Tollestrup, K. Yonehara, M.G. Collura, R.P. Johnson, IPAC13, TUPF1064

[5] V. Kashikhin, V.S. Kashikhin, M.J. Lamm, M.L. Lopes, A.V. Zlobin, M. Alsharo'a, R.P. Johnson, S.A. Kahn, EPAC08, WEPD015

[6] G.M. Kazakevich, G. Flanagan, R.P. Johnson, F. Marhauser, M.L. Neubauer, B. Chase, S. Nagaitsev, R.J. Pasquinelli, N. Solyak, V. Tupikov, D. Wolff, V.P. Yakovlev, IPAC12, WEPPC059

[7] T. Roberts, g4beamline.muonsinc.com

[8] K. Yonehara, R.P. Johnson, M. Neubauer, Y. S. Derbenev, IPAC10, MPPD076

[9] C. Yoshikawa, 2013 UCLA Higgs Factory Workshop hepconf.physics.ucla.edu/higgs2013/talks/yoshikawa. pdf

[10] P. Hanlet, M. Alsharo'a, R.E. Hartline, R.P. Johnson, M. Kuchnir, K. Paul, C. M. Ankenbrandt, A. Moretti, M. Popovic, D. M. Kaplan, K. Yonehara, EPAC06, TUPCH147

[11] K. Yonehara, M.Chung, A. Tollestrup, R.P. Johnson, T.J.Roberts, R.D.Ryne, B.Freemire, R. Samulyak, IPAC13, TUPF1058

[12] K. Yonehara, M. Chung, M.R. Jana, M. Leonova, A. Moretti, A. Tollestrup, R.P. Johnson, B. Freemire, Y. Torun, P. Hanlet, IPAC13, TUPF1059

[13] L.M. Nash, M. Leonova, A. Moretti, M. Popovic, A. Tollestrup, K. Yonehara, G. Flanagan, R.P. Johnson, F. Marhauser, J.H. Nipper,Y. Torun, IPAC13, TUPF1068

[14] G.M. Kazakevich, G. Flanagan, R.P. Johnson, F. Marhauser, M.L. Neubauer, B. Chase, S. Nagaitsev, R.J. Pasquinelli, V.P. Yakovlev, T.A. Treado, IPAC12, WEPPC060

[15] N. Andreev, E. Barzi, G. Chlachidze, D. Evbota, V.S. Kashikhin, V.V. Kashikhin, M.J. Lamm, A. Makarov, I. Novitski, D.F. Orris, M.A. Tartaglia, J.C. Tompkins, D. Torrioni, D. Walbridge, M. Yu, A.V. Zlobin, MT22, 2011, FERMILAB-CONF-11-441-TD

[16] M. Yu, V. Lombardo, M.L. Lopes, D. Turrioni, A.V. Zlobin, G. Flanagan, R.P. Johnson, PAC11, TUP153